Turbulence measurements: An assessment of Acoustic Doppler Current Profiler accuracy in rough environment

Philippe Mercier, Maxime Thiébaut, Sylvain Guillou, Christophe Maisondieu, Emmanuel Poizot, Aline Pieterse, Jérôme Thiebot, Jean-François Filipot, Mikaël Grondeau

Ocean Engineering
April 2021, Volume 226 Pages 108819 (9p.)
https://doi.org/10.1016/j.oceaneng.2021.108819
https://archimer.ifremer.fr/doc/00685/79745/

Turbulence measurements: An assessment of Acoustic Doppler Current Profiler accuracy in rough environment

Mercier Philippe [1, *] , Thiébaut Maxime [2], Guillou Sylvain [1, *], Maisondieu Christophe [3], Poizot Emmanuel [1, 4], Pieterse Aline [2, 3], Thiébot Jérôme [1], Filipot Jean-Francois [2], Grondeau Mikaël [1]

[1] Normandie Université, UNICAEN LUSAC, EA 4253, 60 rue Max Pol Fouchet, CS 20082, 50130 Cherbourg-en-Cotentin, France
[2] France Energies Marines, 525 avenue Alexis de Rochon, 29280 Plouzané, France
[3] Institut Français de Recherche pour l'Exploitation de la Mer, 1625 route de Sainte-Anne CS 10070, 29280 Plouzané, France
[4] Cnam-Intechmer, Boulevard de Collignon, 50110 Cherbourg-en-Cotentin, France

* Corresponding authors : Philippe Mercier, email address : philippe.mercier@unicaen.fr ; Sylvain Guillou, email address : sylvain.guillou@unicaen.fr

Abstract :

The deployment of tidal turbines requires a precise hydrodynamic characterisation of the production site. Acoustic Doppler Current Profilers (ADCP), usually employed for measuring the time-mean characteristics of environmental flows, could also be used for assessing the main features of turbulence. ADCP measurements are sensitive to many sources of uncertainties associated mainly with the spreading of the beams or the assumptions made on flow homogeneity. The ability of ADCPs to accurately measure the hydrodynamic parameters of a given flow can be tested on a synthetic dataset. However, it is difficult to generate a dataset representative of a real environmental flow. In this work, large-eddy simulation of a high Reynolds flow over a rough seabed is performed and used to assess the accuracy of two, coupled, 4-beam ADCP systems forming an 8-beam arrangement. The study confirms the relevance and efficiency of the tested 8-beam configuration for the characterisation of turbulence. The results near the seabed are of a lower quality, with up to 50 % error on the Reynolds stresses for elevations under twice the roughness height, which questions the interpretation of ADCP measurements in the lower part of the water column. Also, the spatial averaging over ADCP cells leads to an underestimation of the turbulence intensity of 10 % to 20 %.

Highlights

► Virtual ADCP measurements are performed on a synthetic LES flow over a rough seabed. ► The use of coupled ADCPs for the measurement of the full Reynolds tensor is validated. ► The Reynolds stresses are underestimated due to the spatial averaging over ADCP cells. ► The quality of ADCP measurements is reduced in the rough boundary layer.

Keywords : Turbulence, Lattice Boltzmann Method, Large-Eddy Simulation, ADCP, Environmental flows

1. Introduction

Tidal power constitutes a potential new source of low carbon power. Although the tidal industry is still in a development phase, real scale prototypes are being tested in operating conditions (e.g., Simec Atlantis and Andritz Hydro turbines in the Pentland First, Sabella turbine in Passage du Fromveur, Hydroquest turbine in Paimpol-Bréhat). As tidal power farms will be composed of arrays of devices distributed over relatively large areas, the optimal layout will depend, for a large part, on the characteristics of the hydrodynamics and the variability of the flow in time and space. Regional tidal flow simulations provide accurate estimates of flow intensity and direction [Thiébot et al. (2020); Lewis et al. (2015); Thiébaut et al. (2019)]. However, these studies are based on Reynolds averaged numerical simulations, that only resolve the time-mean flow and model the effect of turbulence. Although they allow for estimating the turbulence intensity [Togneri et al. (2017b)], they do not simulate turbulent eddies and are limited in terms of spatial and temporal resolutions. Following the work of [Finnegan et al. (2020)], four main aspects have been identified that contribute to unsteady loads on tidal turbine blades and their premature fatigue: the cyclic loading of a blade linked to the vertical gradient of velocity in the swept area, the shadow effects from the support structure, the force due to the sea surface waves [Lewis et al. (2014)] and the force

due to ambient turbulence. As incoming turbulence is an important source of mechanical constraints on tidal turbines [Thiébaut et al. (2020b); Milne et al. (2016)] and impacts turbine wakes [Grondeau et al. (2019)], its characterisation is essential [Milne et al. (2016)]. The power production is stable over long periods of time [Lewis et al. (2019)], however, turbulence might generate electrical surges that need to be anticipated to preserve the power system. Several Large-Eddy Simulations (LES) have been performed, such as [Zangiabadi et al. (2015)] in the Ramsey Sound, [Bourgoin et al. (2020)] and [Mercier et al. (2020a)] in the Raz Blanchard, and [Le et al. (2018)] in the Mississippi River. These simulations enable the assessment of turbulence metrics, such as the full Reynolds tensor, but are limited in resolution, temporal and spatial coverage.

In situ measurements are widely used to estimate the local turbulence metrics [Thomson et al. (2010)]. Bottom mounted Acoustic Doppler Current Profilers (ADCPs) are commonly used for flow characterisation in situations where simultaneous velocity measurements are desired throughout the water column, to investigate the vertical distribution of the current velocities. ADCPs use the Doppler shift in the echoes of a pulsed signal along directed acoustic diverging-beams to estimate flow velocities. Such sensors can be deployed in various environments such as oceans, rivers or estuaries and for long intervals of time (several months), allowing for an assessment of the flow variability over a wide range of time scales, with a typical sampling frequency of a few hertz. They can be employed for an extensive range of applications and especially for turbulence characterisation [McMillan et al. (2016); Guerra et al. (2017); Thiébaut et al. (2020a)]. Velocity fluctuations derived from ADCP measurements enable the quantification of several characteristics of the turbulent kinetic energy (TKE) budget such as the TKE dissipation and TKE production rate, as well as the diffusive transport term [Thiébaut et al. (2020c)].

The use of 4-beam ADCPs for turbulence characterisation gained popularity since [Lohrmann et al. (1990)] introduced the so-called variance method. With this technique, profiles with two components (out of six) of the Reynolds stress tensor are estimated from along-beam velocity measurements, using the difference between the velocity variances along opposing beams [Lu and Lueck (1999); Stacey et al. (1999); Rippeth et al. (2003)]. In comparison to 4-beam ADCPs, 5-beam ADCPs allow for a true measurement of vertical velocities and the estimation of five components of the Reynolds stress tensor [Guerra et al. (2017)], and reduce wave disturbances [Togneri et al. (2017a)].

Recently, 7-beam ADCPs have emerged [Droniou et al. (2019)], enabling the full Reynolds stress tensor to be solved but they still require development and validation. A valuable alternative to 7-beam ADCPs, for fully resolving the Reynolds stress tensor, is the combination of two 4-beam ADCPs [Vermeulen et al. (2011)]. The data from the eight beams allow the six components of the tensor to be resolved. Recently, this method has been implemented to coupled ADCP measurements performed in the Goulet de Brest, France [Pieterse et al. (2017)] and in the Raz Blanchard [Thiébaut et al. (2020c,b)].

One of the main limitations of ADCPs when it comes to turbulence characterisation is the assumption of the homogeneity of the flow field over the measurement volume. Indeed, such sensors use beams that diverge away from the sensor. Hence, the volume in which the flow is assumed homogeneous and in which the measurements are being integrated, increases, changing the spatial averaging of the flow characteristics. Although this homogeneity assumption is widely applied, its validity is likely to fail in particular flow conditions.

An analytical study of the ADCP functioning allows to assess their limits [Guion and Young (2014)]. However, such an analysis does not take into account the specificity of a realistic flow field, and in particular the potential spatial variability of the flow characteristics. The validity of ADCP data processing can be assessed through Virtual-ADCP (V-ADCP) methods, which consists in applying ADCP data processing to a controlled flow field generated analytically [Crossley et al. (2017)] or by numerical simulation [Tokyay et al. (2009); Richmond et al. (2015)]. The velocity field should be representative of the studied environmental flow. In particular, the impact of realistic rough seabed morphology on the turbulent characteristics and on the related accuracy of the data processing method has not, to the authors' knowledge, been addressed yet.

The seabed roughness is known to impact the flow characteristics [Hama (1954); Schlichting (1979);

Schindler and Ackerman (2010)]. The structure of flows over a rough seabed is characterised by a rough sub-layer, in which individual roughness wakes induce three-dimensional variations in the flow characteristics. The thickness of this layer is typically two to five time the roughness height [Nikuradse (1950); Perry et al. (1969)], in such a way that in high seabed roughness areas, ADCP measurement validity could be questioned in a large part of the water column. A specific study of the rough sub-layer and its impact on ADCP measurement accuracy in typical tidal power flows is thus necessary.

The structure of environmental flows can be addressed through canopy flow studies, in which roughness is represented by macro-roughness distributions. Uniform distributions of wall-mounted cubes have been investigated experimentally by [Florens et al. (2013); Basley et al. (2019)] and numerically by [Coceal et al. (2007); Anderson et al. (2015)]. [Hardy et al. (2016); Jiang and Liu (2018)] also performed experimental and numerical analyses of flows over a pebble bed. [Ikhennicheu et al. (2018, 2019, 2020); Mercier et al. (2020b)] experimentally and numerically investigated the flow over combinations of real seabed elements such as big rocks or abrupt changes of seabed elevation. However, these studies are limited to moderate Reynolds numbers ($Re \approx 10^6$), which is not representative of flows at tidal energy sites ($Re \approx 10^8$). To conduct numerical simulations at high Reynolds number, the choice of the numerical method is crucial to handle large and complex simulation domains. The Lattice Boltzmann Method (LBM) is an unsteady computational fluid dynamic method based on the resolution of the Boltzmann equation [Bhatnagar et al. (1954); Qian et al. (1992)]. It is well suited to large and complex geometries [Succi et al. (1989)] and can be combined with LES [Smagorinsky (1963); Eggels and Somers (1995)] in order to resolve a large part of the turbulence energy spectrum and to investigate the motion of the largest eddies [Sagaut (2006)] (those that contain most of the turbulent energy and control most of the momentum transfer and turbulent mixing). For these reasons, LBM-LES has been used for environmental numerical simulations [Parmigiani (2013); Mercier et al. (2020a)].

Here, LBM-LES is chosen to perform a simulation of a channel flow over a uniform distribution of wall-mounted cubes, designed to be representative of a tidal energy site. The V-ADCP method is performed on the simulation output to test the accuracy of the ADCP configuration proposed by [Vermeulen et al. (2011)]. Firstly, the numerical simulation method is presented, as well as the ADCP configuration and principles of the V-ADCP method. Then, the simulation results are exploited to investigate the sources of error. Finally, the prospects and limits of the method are discussed.

2. Methods

2.1. Numerical flow simulation

Simulations are performed with the LBM [Bhatnagar et al. (1954); Qian et al. (1992)], a full description of which can be found in [Guo and Shu (2013)]. The code is based on Palabos, a C++ library [url]. LES relies on the static Smagorinsky model [Smagorinsky (1963)], with a Smagorinsky constant of 0.14. The discretisation scheme is D3Q19, and the collision operator relies on the work of [Latt and Chopard (2006)]. A no-slip boundary condition is used at the seabed, based on the work of [Bouzidi et al. (2001)]. Periodic boundary conditions are applied at the longitudinal and lateral boundaries. A free-slip boundary condition is applied at the water surface position. The simulation domain is 320 m long, 80 m wide and 40 m deep. The seabed is composed of 3 m-large cubic elements disposed regularly over the bottom (see Figure 1). This macro-roughness aims at generating a vertical variation of the turbulence intensity similar to that measured with two, coupled, 4-beam ADCPs in the Raz Blanchard [Thiébaut et al. (2020b)], where the mean vertical profile of longitudinal turbulence intensity ranged from 12% near the surface to 21% near the ADCPs at the seabed.

As the domain is periodic, the load losses tend to decrease the flow velocity. This effect is offset by a longitudinal volume force that sustains the flow. The time step is 0.010 s. The mesh resolution is 0.21 m near the seabed and 0.42 m near the water surface. The domain contains 28.3 million cells. The average longitudinal speed is 3 $\mathrm{m.s^{-1}}$ for a volume force corresponding to a 2.5×10^{-3} $\mathrm{m.s^{-2}}$ acceleration. The instantaneous longitudinal velocity along a vertical longitudinal plane is shown in Figure 2. The

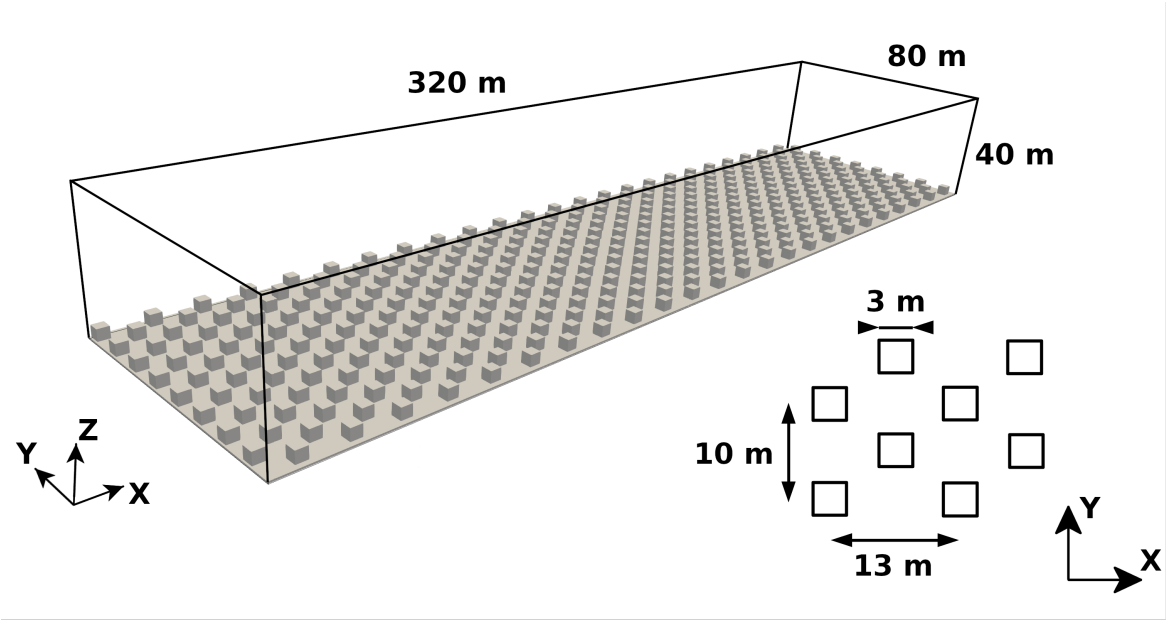

Figure 1: Domain dimensions and cube arrangement.

simulation ran on 56 processors for 78 h. The total simulated time is 52 min, with a convergence period of 36 min. For *in situ* measurements, the period of data extraction must be long enough to guarantee a sufficient number of samples, and short enough not to be affected by changes in the hydrodynamic conditions relative to the tidal cycle. This condition is satisfied by using a 10 min period in the case studied in the work of [Thiébaut et al. (2020b)]. Here, as there is no variation in the hydrodynamic conditions, the period is extended to 16 min. Longitudinal, lateral and vertical velocity components are respectively referred to as u, v and w, acting in the x, y and z directions. Herein, time averaged ($\overline{u}$) and time fluctuating (u') velocities are defined in such way that $u = \overline{u} + u'$.

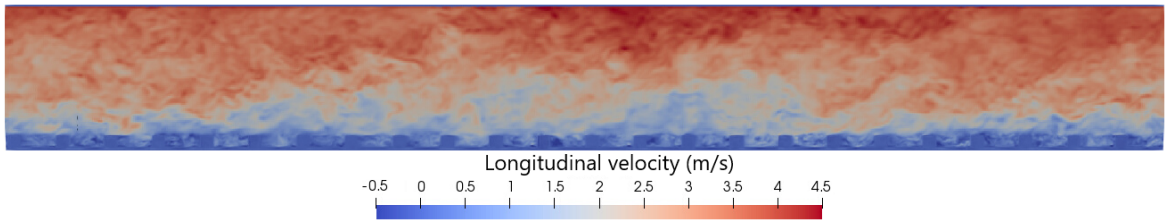

Figure 2: Isosurfaces of instantaneous longitudinal velocity. LBM simulation of a turbulent flow in conditions representative of the hydrodynamics of the Raz Blanchard. Seabed composed of cubic macro-roughness. Image dimensions: 320 m x 40 m.

2.2. Virtual-ADCPs

In the present work, the two, coupled, 4-beam ADCP configuration designed by [Vermeulen et al. (2011)] is tested. This configuration is specially conceived for turbulence measurements. Its working principle is described hereinafter. The V-ADCPs are modelled to represent the sampling geometry of the coupled ADCPs in the representative velocity field derived from the numerical flow simulation. Two upward-looking 4-beam V-ADCPs coupled in a master-slave set-up, are positioned on the seabed forming an 8-beam arrangement where the beams are numbered from 1 to 8 (Figure 3). The two V-ADCPs are at a distance of 0.5 m from each other. The V-ADCPs record alternatively the velocities in beam coordinates (radial velocities) at the frequency rate of 2 Hz.

The angle θ between the transducers and the vertical is 20°, in accordance with the 4-beam ADCPs used in [Vermeulen et al. (2011); Thiébaut et al. (2020c,b)]. A Cartesian coordinate system ($\mathcal{O}$, x, y, z)

is defined relative to the master V-ADCP, with the origin $\mathcal{O}$ located at the centre of the four transducers (Figure 3). The orientation of the master V-ADCP is such that the opposite beams 1 and 2 are oriented along the direction of the longitudinal velocity u, defining the x-axis, whereas beams 3 and 4 are oriented along the direction of the lateral velocity v, defining the y-axis. The slave V-ADCP is rotated to an angle $\phi_1 = 20^{\circ}$ around the x-axis (Figure 3), and $\phi_3 = 45^{\circ}$ around the z-axis resulting in a tilted V-ADCP with one beam pointed vertically upward (Figure 4). No rotation is applied around the y-axis ($\phi_2 = 0^{\circ}$).

The coupled ADCP method, developed by [Vermeulen et al. (2011)], combines (i) the traditional transformation method, where two opposite beams of the ADCP are used to transform velocities in beam coordinates to velocities in Cartesian coordinates, with (ii) the rotation of the slave relative to the master ADCP. The velocities in beam coordinates equates to the velocities (u, v, w) in Cartesian coordinates as in Equation 1:

$$\mathbf{b} = T.\mathbf{u} \tag{1}$$

where $\mathbf{b}$ is an eight-component vector containing all the radial velocity components from the two coupled ADCPs, $\mathbf{u}$ is the velocity vector in the Cartesian coordinate system ($\mathbf{u} = u\vec{e_x} + v\vec{e_y} + w\vec{e_z}$) and T is the transformation matrix involving sines and cosines of θ, ϕ_1, ϕ_2 and ϕ_3 [Vermeulen et al. (2011); Thiébaut et al. (2020c,b)]. The velocities in the Cartesian coordinate system are obtained by inverting the transformation matrix, T.

In order to obtain the components of the Reynolds stress tensor from the velocity variances in beam coordinates, a new eight by six matrix, Q, is computed resulting from the product of the terms in T [Vermeulen et al. (2011); Thiébaut et al. (2020c,b)]. The vector $\mathrm{v_b}$ containing the velocity variances in beam coordinates is written as the product of Q by the vector $\mathbf{r}$ containing the six terms of the Reynolds stress tensor, as in Equation 2:

$$\mathrm{v_b} = Q.\mathbf{r} \tag{2}$$

The six-element vector $\mathbf{r}$ can be rearranged to form the Reynolds stress tensor according to Equation 3:

$$\mathbf{r} = \begin{pmatrix} r_1 & r_4 & r_5 \\ r_4 & r_2 & r_6 \\ r_5 & r_6 & r_3 \end{pmatrix} = \begin{pmatrix} \overline{u'^2} & \overline{u'v'} & \overline{u'w'} \\ \overline{u'v'} & \overline{v'^2} & \overline{v'w'} \\ \overline{u'w'} & \overline{v'w'} & \overline{w'^2} \end{pmatrix} \tag{3}$$

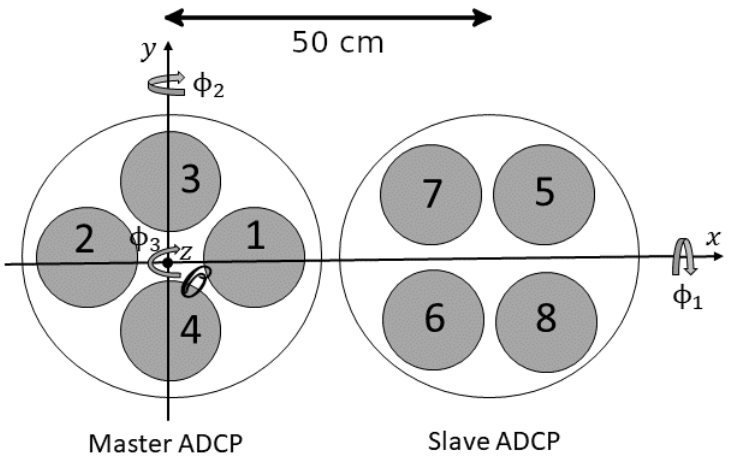

Figure 3: Position and orientation of two coupled 4-beam ADCPs [Vermeulen et al. (2011)].

The Reynolds stresses indicate the orientation of the eddies in the flow and are often used to estimate fundamental turbulence metrics such as the turbulence intensity, the TKE dissipation rate or the TKE

production rate. Here, the $\overline{u'u'}$, $\overline{v'v'}$ and $\overline{w'w'}$ components will be referred to as normal stresses and the $\overline{u'v'}$, $\overline{u'w'}$ and $\overline{v'w'}$ components as the shear stresses.

V-ADCP cells are defined by all the mesh nodes included in a volume delimited by a frustum of 4° beam cone. The cells of the master and slave V-ADCP are respectively 1.28 m and 1.37 m thick. This corresponds to the configuration used in [Thiébaut et al. (2020c)]. The cells are presented in Figure 4. They are composed of a number of mesh nodes ranging from 4 to 135 and their volume ranges from 0.5 m^3 to 17 m^3, depending on their elevation. Similarly to real ADCPs, the spatial averaging of the radial velocity is performed on each cell volume. This process is replicated on each V-ADCP beam. The issue of Doppler noise [Brumley et al. (1991)] and other practical operational considerations are ignored. Also, if the acquisition frequency affects the consideration of the smallest scales of the turbulence in standard ADCP uses [Guion and Young (2014)], it is not the case for data processing based on the variance method. Thus, this matter is not addressed here.

The Reynolds stresses are computed directly from the synthetic flow field on a vertical profile centred on the master V-ADCP position, with a high frequency data acquisition (100 Hz). This dataset will be referred to as the reference dataset. Simultaneously, the Reynolds stresses are calculated from the velocities recorded by the V-ADCP. The comparison between Reynolds stresses derived from both methods will allow for the assessment of the error inherent to ADCP measurements.

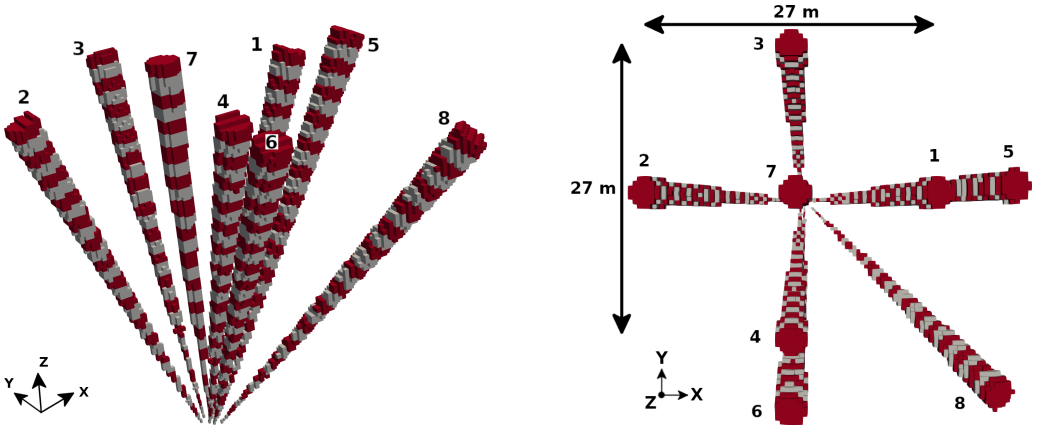

(a) Side view. (b) Plan view.

Figure 4: Visualisation of the eight beams of the V-ADCP configuration. Each alternate grey and red stripe corresponds to an individual cell.

3. Results

3.1. Comparison of Reynolds stresses derived from the reference dataset and V-ADCP

Figure 5 shows scatterplots of the six components of the Reynolds stress tensor derived from the reference dataset and the V-ADCP at each cell elevation. The 1:1 black line indicates perfect agreement between Reynolds stresses derived from both methods.

In general, a good agreement is found, with the $\overline{u'u'}$, $\overline{v'v'}$, $\overline{w'w'}$, $\overline{u'v'}$ and $\overline{u'w'}$ components matching the 1:1 line. However, a few values are found to be significantly far from the 1:1 line, especially in the normal stresses $\overline{u'u'}$ and $\overline{v'v'}$, where these values were calculated near the seabed. Moreover, the component $\overline{v'v'}$ exhibits some inconsistencies with two negative values derived from the V-ADCP.

The scatterplots of the normal stresses ($\overline{u'u'}$, $\overline{v'v'}$ and $\overline{w'w'}$) are slightly right-skewed, indicating that the V-ADCP underestimates these components. Since the normal stresses allow for the calculation of the turbulence intensity, it is expected that the V-ADCP gives underestimated values of this metric. Moreover, the shear stress, $\overline{v'w'}$, is characterised by very low absolute values. This is imputed to the

symmetric characteristic of the domain. The domain symmetry should imply that the $\overline{u'v'}$ component also satisfies this condition, which is not the case.

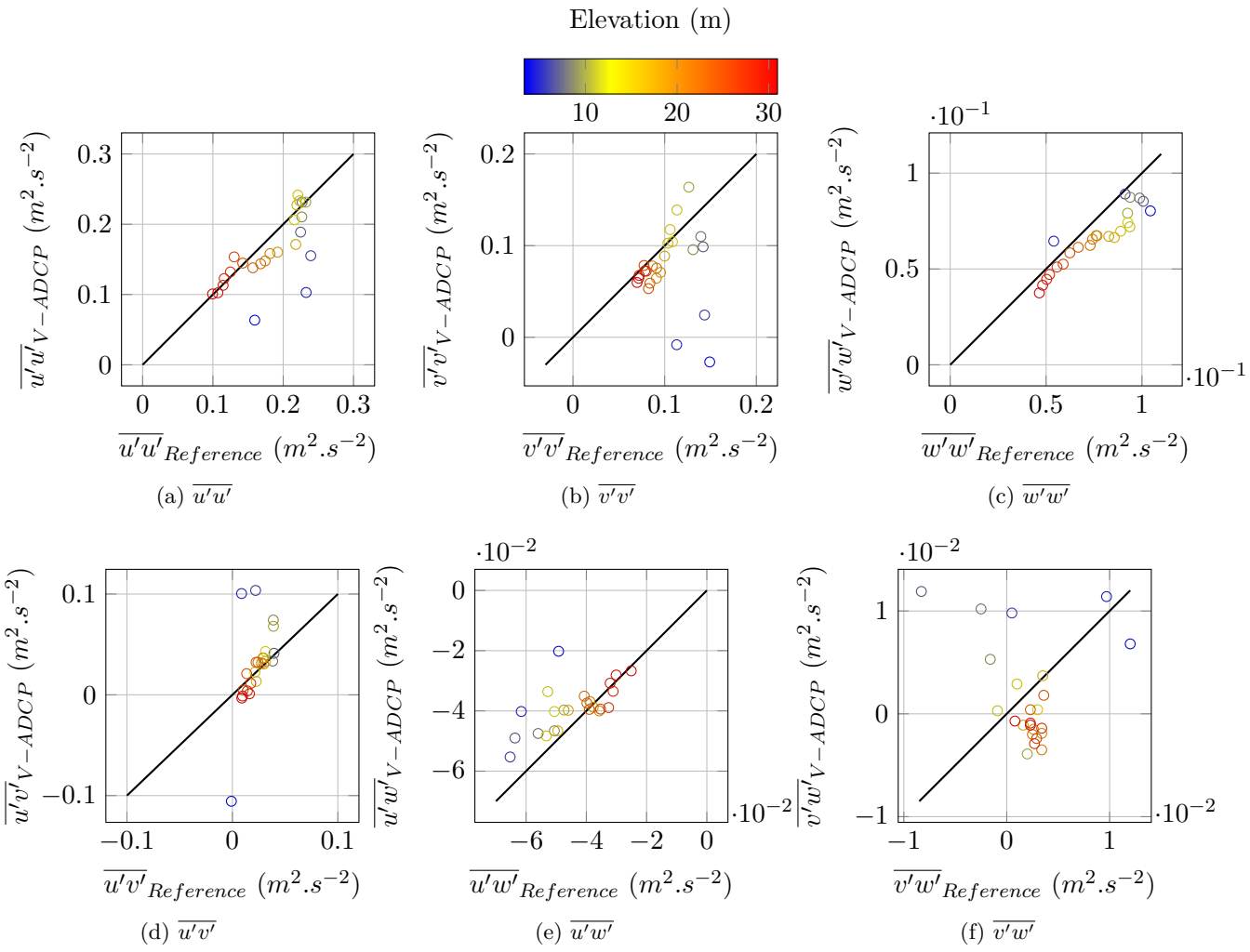

Figure 5: Comparison of the Reynolds stresses derived from V-ADCP and reference data. Each dot stands for a different elevation through the water column, between 3.3 m and 31 m, as shown by the colour bar.

Vertical profiles of the Reynolds stresses are shown in Figure 6. This figure exhibits a good agreement between profiles derived from the reference dataset and V-ADCP. The absolute error is greater near the seabed, which could result from spatial heterogeneity of the flow over a horizontal plane that invalidates the homogeneity assumption. This assumption is necessary for the application of the method proposed by [Vermeulen et al. (2011)] (Section 2.2). However, as demonstrated by [Nikuradse (1950); Perry et al. (1969)], this assumption is true for elevations above 2 to 5 times the roughness height. Therefore, it may not be valid in the lower part of the water column, which induces high error. This is consistent with the high absolute error observed here up to 8 m above the seabed.

The maximum relative error (MaxError - Equation 4) and the root mean square error (RMSE - Equation 5) between the Reynolds stresses derived from the reference dataset and the V-ADCP are shown in Table 1. Only values calculated at a height above seabed higher than 8 m are taken into account. The maximum RMSE is associated with the shear stress $\overline{v'w'}$ with a value of 137 %. This high value is not troublesome as the $\overline{v'w'}$ component is centred on zero. The RMSE of the five other components of the Reynolds stress tensor is relatively low, with values ranging from 8 % to 14 % and up to 33 % for $\overline{u'v'}$.

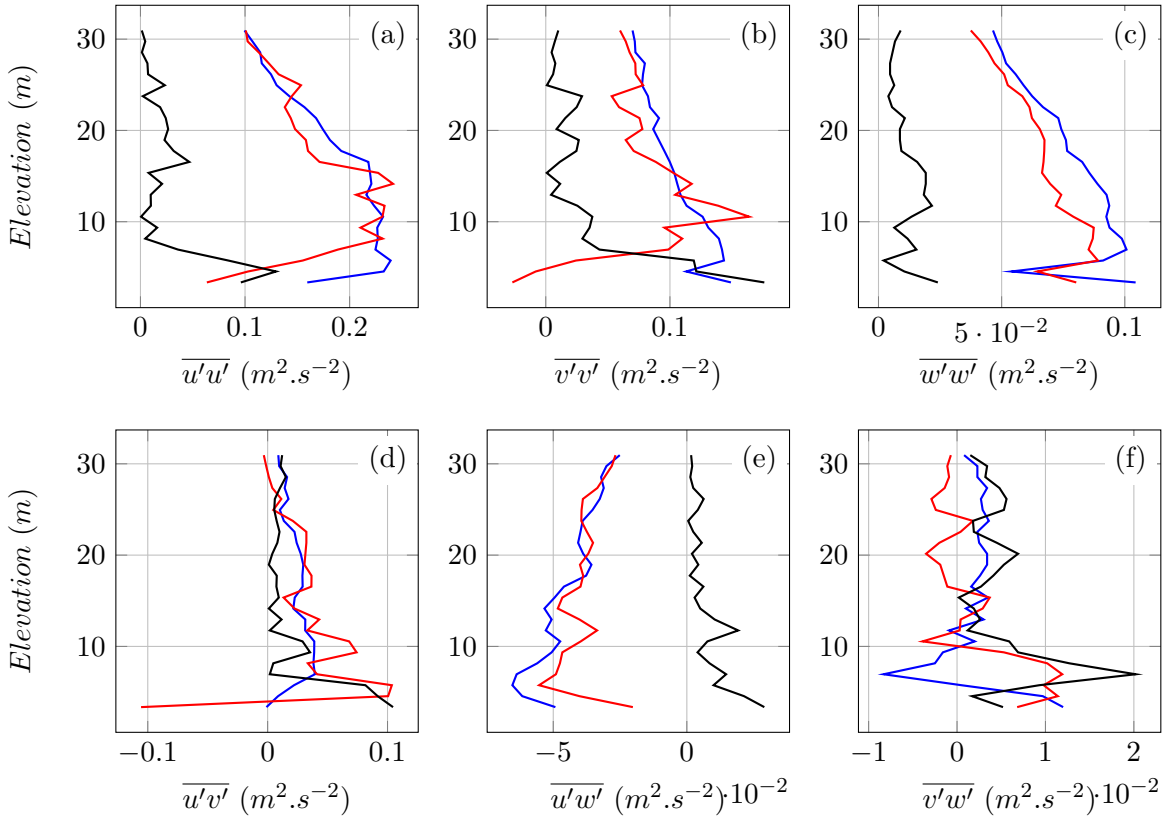

Figure 6: Vertical profiles of the Reynolds stresses derived from the reference dataset (blue —) and the V-ADCP (red —). Black profiles (—) denote the difference between the Reynolds stress estimation from both methods.

	$\overline{u'u'}$	$\overline{v'v'}$	$\overline{w'w'}$	$\overline{u'v'}$	$\overline{u'w'}$	$\overline{v'w'}$
Max relative error (%)	20	27	22	91	34	353
RMSE (%)	8	14	12	33	11	137

Table 1: Max and root mean square relative errors between reference and V-ADCP data for all components of the Reynolds stress tensor above 8 m elevation.

The maximum relative error varies over a wide range, with the three components, $\overline{u'u'}$, $\overline{v'v'}$ and $\overline{w'w'}$ associated with maximum relative error lower than 27 % whereas the $\overline{u'v'}$ and $\overline{u'w'}$ components exhibit maximum values of 91 % and 34 % respectively. The component, $\overline{v'w'}$ reveals considerable maximum error reaching 353 %, which is, once again, explained by the fact that the $\overline{v'w'}$ component is centred on zero.

$$\text{MaxError}(X) = 100\frac{\max(|X_{ref} - X_{V-ADCP}|)}{\max(|X_{ref}|)} \tag{4}$$

$$\text{RMSE}(X) = 100\frac{\sqrt{\int_\Omega \frac{(X_{ref}-X_{V-ADCP})^2}{L} d\omega}}{\max(|X_{ref}|)} \tag{5}$$

3.2. Assessment of turbulence homogeneity over the beams

The operating principle of the coupled 4-beam ADCP system requires the inherent assumption of homogeneity in the flow within the sampled area. The reference dataset computed from the synthetic

flow field allows for the direct determination of the vertical evolution of the Reynolds stresses along each beam of the V-ADCPs (Figure 7). It is thus possible to perform a turbulence homogeneity test over the beams.

Figure 7 shows that, for a given component of the Reynolds stress tensor, the profiles derived from each V-ADCP beam have the same behaviour. Their magnitude increases abruptly up to an elevation of 8-10 m and decreases above 10 m up to the maximum elevation. The only component that confirms the turbulence homogeneity assumption throughout the water column is the normal stress $\overline{w'w'}$. For the components $\overline{v'v'}$ and $\overline{u'w'}$ the assumption is not valid for elevations higher than 15 m and 20 m, respectively. The normal stress, $\overline{u'u'}$ reveals two ranges in elevation where the homogeneity assumption may be validated: (i) - from 0 to 8 m and, (ii) - from 20 to 38 m (the maximum elevation). Between both layers, the Reynolds stress profiles can be split into three groups of beams. The first group is composed of beams 1, 2, 5 and 7, where these beams are aligned with the flow direction. In this direction, the turbulence is homogeneous and rapidly advected. The second group is composed of beams 4, 6 and 8, whose associated profiles exhibit similar behaviour. These beams share the same three-dimensional spanning area (Figure 4). Thus, as expected, these beams capture comparable turbulence processes. Beam 3 spans a different area and constitutes the last group. This decomposition in three groups is particularly noticeable for the component $\overline{u'v'}$, throughout the water column.

Figure 8a shows the vertical profiles of the Reynolds stresses derived from the reference dataset and averaged over the 8 beams. The profiles used to calculate and normalise the average gap between individual and spatially averaged beams are represented in Figure 8b. For $\overline{u'u'}$, $\overline{v'v'}$, $\overline{w'w'}$ and $\overline{u'w'}$ components, the discrepancies are high in the lower part of the water column (up to 10 m), low in the medium part of the water column and increase between 20 m and the maximum elevation. For $\overline{u'v'}$ and $\overline{v'w'}$ the same tendency is observed but with higher magnitudes. The origin of the discrepancies in the lower part of the water column can be explained by the presence of seabed roughness that is expected to affect the homogeneity of the flow up to 2 to 5 times its height (6 m to 15 m). Discrepancies observed in the upper part of the water column could be explained by increasing distance between V-ADCP beams, potentially reducing the validity of the assumption made on the horizontal homogeneity of the flow.

3.3. Effect of spatial averaging inside V-ADCP cells

Similarly to real ADCPs, the velocities derived from the V-ADCPs were averaged over each bin cell volume. This spatial averaging is expected to filter small eddies, thus affecting the evaluation of turbulence metrics. This filtering effect can be assessed through numerical simulation, because the full velocity vector is accessible at a high spatial resolution. In order to investigate the potential filtering-induced biases when characterising turbulence, the reference dataset, extracted from individual simulation nodes, are compared to the data averaged over each cell of the 7th beam of the V-ADCPs (Figure 9). This beam is oriented vertically upward and matches the position of the vertical reference profile. The vertical evolution of the Reynolds stresses derived from both the reference dataset and the V-ADCPs are similar. However, the V-ADCP data significantly and systematically underestimates the magnitude of the Reynolds stresses, especially for the normal stresses. This result is in agreement with the right-skewed distribution of the scatterplots associated with the normal stresses presented in Figure 5. For each component, the difference is more significant in the lower part of the water column and ranges from 10 % to 20 %.

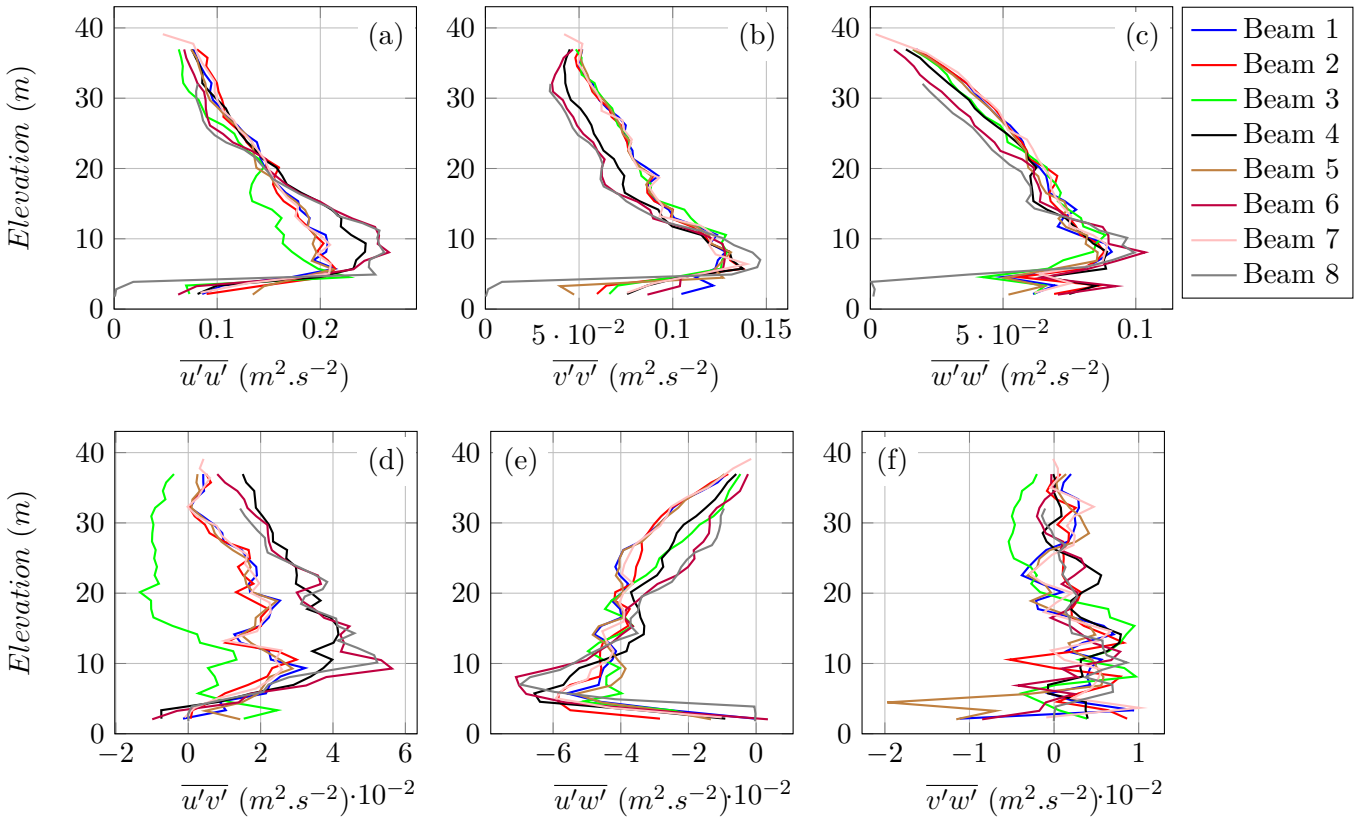

Figure 7: Vertical profiles of the Reynolds stresses derived from the reference dataset along each beam of the V-ADCP.

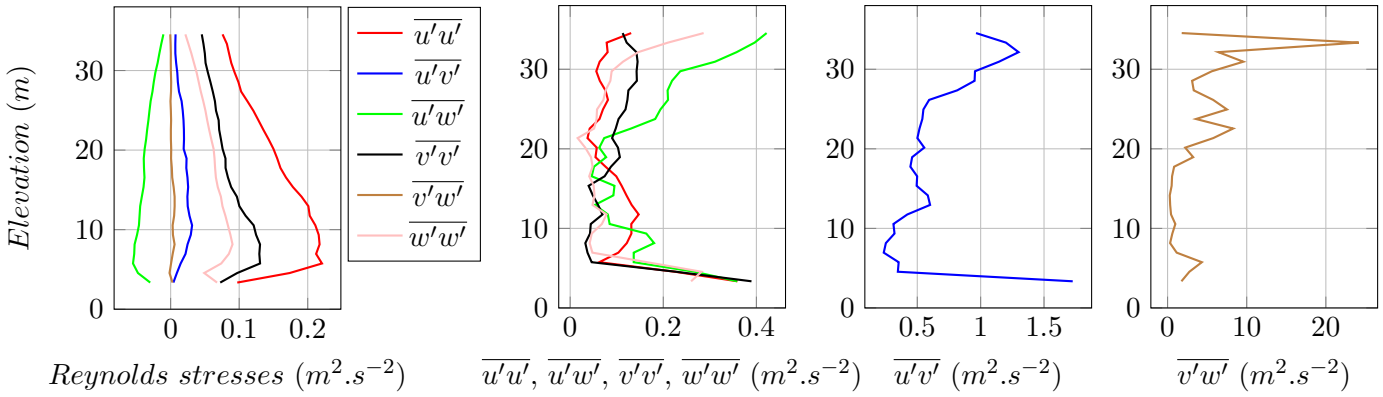

(a) Average over 8 beams.

(b) Normalised average difference with the average value.

Figure 8: Evaluation of the dispersion of Reynolds stresses over the 8 V-ADCP beams.

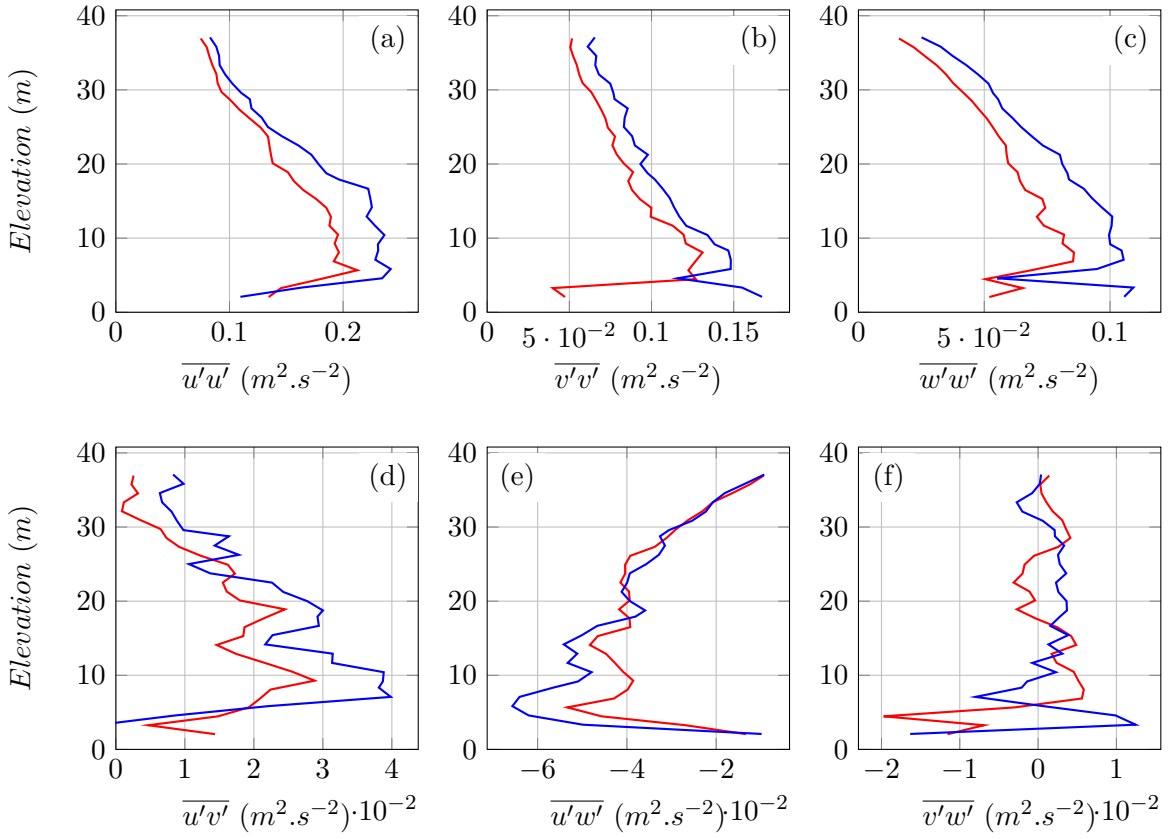

Figure 9: Comparison of the Reynolds stress calculated from beam number 7 (in red) and the reference dataset (in blue).

4. Conclusion

In this study, the ability of a coupled 4-beam ADCP system to characterise the six components of the Reynolds stress tensor is assessed. LES of high Reynolds flow over a rough bed is performed in order to build a reference synthetic dataset used to directly estimate the Reynolds stresses. The coupled ADCP system (V-ADCP) is assumed to be located on the seabed measuring the along-beam velocities of the synthetic flow [Vermeulen et al. (2011)]. The Reynolds stresses derived from the V-ADCPs are estimated following the methodology proposed by [Thiébaut et al. (2020c,b)].

Comparison between Reynolds stresses derived from both the reference dataset and the V-ADCPs are generally in good agreement. The flow heterogeneity over the ADCP beams and the spatial averaging over ADCP cells are found to be the two main sources of error in the interpretation of ADCP measurements.

Flow heterogeneity is observed in the lower part of the water column, where the seabed roughness wakes have a local influence on the turbulence metrics. It is significant up to twice the roughness height (6 m). This leads to high discrepancies between V-ADCP and reference results. As a consequence, ADCP measurements should be interpreted with caution near the seabed in the case of a high seabed roughness.

Flow heterogeneity is also observed in the upper part of the water column, where the distance between beams increases. The heterogeneity is observed in the lateral direction and not in the longitudinal direction. Indeed, the transport of turbulence characteristics in the longitudinal direction is expected to be faster than its diffusion in the lateral direction, resulting in a higher homogeneity in the longitudinal direction than in the lateral direction. However, this heterogeneity is expected to have a minor effect on the accuracy of the measurements, since Reynolds stresses derived from the reference dataset and the V-ADCPs are found to be consistent.

The spatial averaging over the cells in the numerical model is found to underestimate the Reynolds stresses by 10 % to 20 %, in particular the normal components which are used to estimate the turbulence intensity. The spatial averaging is performed to simulate the working principle of a real ADCP. However, for this type of sensor, the averaging is not uniform over the cells. Instead, the cells are most sensitive to velocities at their centre and least sensitive at the edges. The velocity in each depth cell is a weighted average using a triangular weighting function. This is not considered in the present study.

These insights could help reducing uncertainties and systematic bias of *in situ* measurements and thus improve the knowledge about environmental flows. This improvement would benefit turbine manufacturers in the optimisation of turbine design.

This work is based on a unique simulation configuration characterised by its flow velocity, size and spacing of roughness and water column height. These conditions are representative of flows at typical tidal energy sites, where the general conclusions of this work would apply. Nevertheless, it is expected that different types of flow would potentially lead to different conclusions.

Real seabed morphology is diversified, as well as environmental flow characteristics. The flow obtained in this study from an idealised seabed roughness cannot be assumed to be representative of all environmental flows. Thus, the conclusions of the present work must be put into perspective with the actual seabed and hydrodynamic conditions of any other specific studied site.

V-ADCPs do not take all biases into account. Numerical simulations are an idealised environment that do not include physical processes leading to the acquisition of data outliers. The conclusions proposed here, give insight for quantifying some sources of error but do not exonerate from usual corrections and uncertainties applied in ADCP measurements such as the bias in turbulence measurements induced by the Doppler noise.

For future work, new simulations could be conducted, using different seabed geometries, water depth and averaged velocity magnitudes. This would help in understanding the effect of these parameters on the accuracy of the tested ADCP configuration and provide more insight into the interpretation of real ADCP measurements. V-ADCPs could be implemented with more detailed numerical models to take

into account physical phenomena that are neglected in this study (such as spatial averaging over an ADCP cell). This would improve the fidelity of V-ADCP data acquisition with respect to real ADCPs and reinforce the relevance of the conclusions and prescriptions obtained from V-ADCP analysis. Also, the V-ADCP method could be used, not only for turbulence measurements, but also for average velocity measurements. In particular, it could be used to assess the potential improvement brought by ADCPs based on higher acquisition frequencies. Finally, the simulation of realistic environmental flows combined with the V-ADCP method could help testing new ADCP beam configurations. The sensitivity of the measurements to the number of beams, beam orientations, cell thickness or acquisition frequency could be assessed to optimise these parameters for measurements performed in specific environments.

Acknowledgments

This work benefits from a French State grant managed by the National Research Agency under the Investments for the Future program bearing the reference ANR-10-IEED-0006-11 and is also funded by the INTERREG TIGER project. The authors acknowledge the financial support of CD50 and Région Normandie. We are grateful to the CRIANN ("Centre Régional Informatique et d'Applications Numériques de Normandie") for providing computational means.

References

http://palabos.unige.ch/. 2.1

W. Anderson, Q. Li, and E. Bou-Zeid. Numerical simulation of flow over urban-like topographies and evaluation of turbulence temporal attributes. Journal of Turbulence, 16:809–831, 2015. URL http://dx.doi.org/10.1080/14685248.2015.1031241. 1

J. Basley, L. Perret, and R. Mathis. Structure of high Reynolds number boundary layers over cube canopies. Journal of Fluid Mechanics, 870:460–491, 2019. URL https://doi.org/10.1017/jfm.2019.274. 1

P.L. Bhatnagar, E.P. Gross, and M. Krook. A model for collision processes in gases. Physical Review, 94 (3), 1954. URL http://dx.doi.org/10.1103/PhysRev.94.511. 1, 2.1

A. Bourgoin, S. Guillou, J. Thiébot, and R. Ata. Turbulence characterization at a tidal energy site using large-eddy simulations: case of the Alderney Race. Philosophical Transactions of the Royal Society A, 378(20190499), 2020. URL https://doi.org/10.1098/rsta.2019.0499. 1

M. Bouzidi, M. Firdaouss, and P. Lallemand. Momentum transfer of a Boltzmann-lattice fluid with boundaries. Physics of Fluids, 13(3452), 2001. URL https://doi.org/10.1063/1.1399290. 2.1

B.H. Brumley, R.G. Cabrera, K.L. Deines, and E.A. Terray. Performance of a broad-band acoustic Doppler current profiler. IEEE Journal of Oceanic Engineering, 16:402–407, 1991. URL https://doi.org/10.1109/48.90905. 2.2

O. Coceal, A. Dobre, and T.G. Thomas. Unsteady dynamics and organized structures from DNS over an idealized canopy. International Journal of Climatology, 27:1943–1953, 2007. URL http://dx.doi.org/10.1002/joc.1549. 1

G. Crossley, A. Alexandre, S. Parkinson, A.H. Day, H.C.M. Smith, and D.M. Ingram. Quantifying uncertainty in acoustic measurements of tidal flows using a 'Virtual' Doppler Current Profiler. Ocean Engineering, 137:404–416, 2017. URL https://doi.org/10.1016/j.oceaneng.2017.04.015. 1

E. Droniou, M. Folley, Y. Perignon, and C. Boake. Advanced measurement and analysis of waves and turbulence using 5-, 7- or 8-beam ADCPs. In Proceedings of the 13th European Wave and Tidal Energy Conference 1-6 Sept 2019, Naples, Italy, 2019. 1

J.G.M. Eggels and J.A. Somers. Numerical simulation of free convective flow using the lattice-Boltzmann scheme. International Journal of Heat and Fluid Flow, 16(5), 1995. URL https://doi.org/10.1016/0142-727X(95)00052-R. 1

W. Finnegan, E. Fagan, T. Flanagan, A. Doyle, and J. Goggins. Operational fatigue loading on tidal turbine blades using computational fluid dynamics. Renewable Energy, 152:430–440, 2020. URL https://doi.org/10.1016/j.renene.2019.12.154. 1

E. Florens, O. Eiff, and F. Moulin. Defining the roughness sublayer and its turbulence statistics. Exp Fluids, 54:1500, 2013. URL http://dx.doi.org/10.1007/s00348-013-1500-z. 1

M. Grondeau, S. Guillou, P. Mercier, and E. Poizot. Wake of a ducted vertical axis tidal turbine in turbulent flows, LBM actuator-line approach. Energies, 12(4273), 2019. URL https://doi.org/10.3390/en12224273. 1

M. Guerra, R. Cienfuegos, J. Thomson, and L. Suarez. Tidal energy resource characterization in Chacao Channel, Chile. International Journal of Marine Energy, 20:1–16, 2017. URL https://doi.org/10.1016/j.ijome.2017.11.002. 1

R.U.G. Guion and A.M. Young. The frequency response of acoustic doppler current profilers: Spatiotemporal response and implications for tidal turbine site assessment. In 2014 Oceans - St. John's, 2014. URL https://doi.org/10.1109/OCEANS.2014.7003057. 1, 2.2

Z. Guo and C. Shu. Lattice Boltzmann Method and its applications in engineering. Advances in Computational Fluid Dynamics, 2013. URL https://doi.org/10.1007/s11434-009-0681-6. 2.1

F.R. Hama. Boundary-layer characteristics for smooth and rough surfaces. In The Society of Naval Architects and Marine Engineers, 1954. 1

R.J. Hardy, J.L. Best, D.R. Parsons, and T.I. Marjoribanks. On the evolution and form of coherent flow structures over a gravel bed: Insights from whole flow field visualiszation and measurement. Journal of Geophysical Research: Earth Surface, 121:1472–1493, 2016. URL https://doi.org/10.1002/2015JF003753. 1

M. Ikhennicheu, B. Gaurier, P. Druault, and G. Germain. Experimental analysis of the floor inclination effect on the turbulent wake developing behind a wall mounted cube. European Journal of Mechanics - B Fluids, 72:340–352, 2018. URL https://doi.org/10.1016/j.euromechflu.2018.07.003. 1

M. Ikhennicheu, G. Germain, P. Druault, and B. Gaurier. Experimental investigation of the turbulent wake past realistic seabed elements for velocity variations characterisation in the water column. International Journal of Heat and Fluid Flow, 78(108426), 2019. URL https://doi.org/10.1016/j.ijheatfluidflow.2019.108426. 1

M. Ikhennicheu, P. Druault, B. Gaurier, and G. Germain. Turbulent kinetic energy budget in a wall-mounted cylinder wake using PIV measurements. Ocean Engineering, 210(107582), 2020. URL https://doi.org/10.1016/j.oceaneng.2020.107582. 1

Y. Jiang and X. Liu. Experimental and numerical investigation of density current over macro-roughness. Environmental Fluid Mechanics, 18:97–116, 2018. URL https://doi.org/10.1007/s10652-016-9500-1. 1

J. Latt and B. Chopard. Lattice Boltzmann method with regularized pre-collision distribution functions. Mathematics and Computers in Simulation, 72:165–168, 2006. URL https://doi.org/10.1016/j.matcom.2006.05.017. 2.1

T.B. Le, A. Khosronejad, F. Sotiropoulos, N. Bartelt, S. Woldeamlak, and P. Dewall. Large-eddy simulation of the Mississippi River under base-flow condition: hydrodynamics of a natural diffluence-confluence region. Journal of Hydraulic Research, 2018. URL https://doi.org/10.1080/00221686.2018.1534282. 1

M. Lewis, S. P. Robins, and M. R. Hashemi. Resource assessment for future generations of tidal-stream energy arrays. Energy, 83:403–415, 2015. URL http://dx.doi.org/10.1016/j.energy.2015.02.038. 1

M. Lewis, J. McNaughton, C. Márquez-Dominguez, G. Todeschini, M. Togneri, I. Masters, M. Allmark, T. Stallard, S. Neilla, A. Goward-Brown, and P. Robinsa. Power variability of tidal-stream energy and implications for electricity supply. Energy, 183:10671–1074, 2019. URL https://doi.org/10.1016/j.energy.2019.06.181. 1

M.J. Lewis, S.P. Neill, M.R. Hashemi, and M. Reza. Realistic wave conditions and their influence on quantifying the tidal stream energy resource. Applied Energy, 136:495–508, 2014. URL http://dx.doi.org/10.1016/j.apenergy.2014.09.061. 1

A. Lohrmann, B. Hackett, and L.P. Røed. High resolution measurements of turbulence, velocity and stress using a pulse-to-pulse coherent sonar. Journal of Atmospheric and Oceanic Technology, 7:19–37, 1990. URL https://doi.org/10.1175/1520-0426(1990)007<0019:HRMOTV>2.0.CO;2. 1

Y. Lu and R.G. Lueck. Using a braodband ADCP in a tidal channel. Part II: Turbulence. Journal of Atmospheric and Oceanic Technology, 16:1568–1679, 1999. URL https://doi.org/10.1175/1520-0426(1999)016<1568:UABAIA>2.0.CO;2. 1

J.M. McMillan, A.E. Hay, R.G. Lueck, and F. Wolk. Rates of dissipation of turbulent kinetic energy in a high Reynolds number tidal channel. Journal of Atmospheric and Oceanic Technology, 33:817–837, 2016. URL https://doi.org/10.1175/JTECH-D-15-0167.1. 1

P. Mercier, M. Grondeau, S. Guillou, J. Thiébot, and E. Poizot. Numerical study of the turbulent eddies generated by the seabed roughness. Case study at a tidal power site. Applied Ocean Research, 97 (102082), 2020a. URL https://doi.org/10.1016/j.apor.2020.102082. 1

P. Mercier, M. Ikhennicheu, S. Guillou, G. Germain, E. Poizot, M. Grondeau, J. Thiébot, and P. Druault. The merging of Kelvin–Helmholtz vortices into large coherent flow structures in a high Reynolds number flow past a wall-mounted square cylinder. Ocean Engineering, 204(107274), 2020b. URL https://doi.org/10.1016/j.oceaneng.2020.107274. 1

I.A. Milne, A.H. Day, R.N. Sharma, and R.G.J. Flay. The characterisation of the hydrodynamic loads on tidal turbines due to turbulence. Renewable and Sustainable Energy Reviews, 56:851–864, 2016. 1

J. Nikuradse. Laws of flow in rough pipes. National Advisory Committee for Aeronautics, 1950. 1, 3.1

A. Parmigiani. A lattice Boltzmann simulation of the Rhone river. International Journal of Modern Physics C, 24(12), 2013. URL https://doi.org/10.1142/S0129183113400081. 1

A.E. Perry, W.H. Schofield, and P.N. Joubert. Rough wall turbulent boundary layers. Journal of Fluid Mechanics, 37:383–413, 1969. URL https://doi.org/10.1017/S0022112069000619. 1, 3.1

A. Pieterse, J.-F. Filipot, C. Maisondieu, L. Kilcher, and N. Chaplain. Coupled ADCP measurements for tidal turbulence characterization. In Proceedings of the 12th European Wave and Tidal Energy Conference, 2017. 1

Y.H. Qian, D. D'Humières, and P. Lallemand. Lattice BGK models for Navier-Stokes equation. Europhysics Letters, 17:479–484, 1992. URL https://doi.org/10.1209/0295-5075/17/6/001. 1, 2.1

M. Richmond, S. Harding, and P. Romero-Gomez. Numerical performance analysis of acoustic Doppler velocity profilers in the wake of an axial-flow marine hydrokinetic turbine. International Journal of Marine Energy, 11:50–70, 2015. URL https://doi.org/10.1016/j.ijome.2015.05.004. 1

T. Rippeth, J.H. Simpson, E. Williams, and M.E. Inall. Measurement of the rates of production and dissipation of turbulent kinetic energy in an energetic tidal flow: Red Wharf Bay revisited. Journal of Physical Oceanography, 33:1889–1901, 2003. URL https://doi.org/10.1175/1520-0485(2003)033<1889:MOTROP>2.0.CO;2. 1

P. Sagaut. Large Eddy Simulation for Incompressible Flows. Scientific Computation, 2006. 1

R.J. Schindler and J.D. Ackerman. The environmental hydraulics of turbulent boundary layers, chapter 5, pages 87–125. Advances in Environmental Fluid Mechanics, 2010. URL https://dx.doi.org/10.1142/9789814293006_0005. 1

H. Schlichting. Boundary layer theory. McGraw-Hill Book Company, 7th edition, 1979. URL https://dx.doi.org/10.1007/978-3-662-52919-5. 1

J. Smagorinsky. General circulation experiments with the primitive equations. Monthly Weather Review, 91(3):99–164, 1963. URL https://doi.org/10.1175/1520-0493(1963)091<0099:GCEWTP>2.3.CO;2. 1, 2.1

M.T. Stacey, S.G. Monismith, and J.R. Burau. Measurements of Reynolds stress profiles in unstratified tidal flow. Journal of Geophysical Research, 104:10933–10949, 1999. URL https://doi.org/10.1029/1998JC900095. 1

S. Succi, E. Foti, and F. Higuera. Three-dimensional flows in complex geometries with the lattice Boltzmann method. Europhysics Letters, pages 433–438, 1989. URL https://doi.org/10.1209/0295-5075/10/5/008. 1

M. Thiébaut, A. Sentchev, and P. Bailly du Bois. Merging velocity measurements and modeling to improve understanding of tidal stream resource in Alderney Race. Energy, 178:460–470, 2019. URL https://doi.org/10.1016/j.energy.2019.04.171. 1

M. Thiébaut, J.-F. Filipot, C. Maisondieu, G. Damblans, R. Duarte, E. Droniou, N. Chaplain, and S. Guillou. A comprehensive assessment of turbulence at a tidal-stream energy site influenced by wind-generated ocean waves. Energy, 191(116550), 2020a. URL https://doi.org/10.1016/j.energy.2019.116550. Submitted to Energy. 1

M. Thiébaut, J.-F. Filipot, C. Maisondieu, G. Damblans, C. Jochum, L.F. Kilcher, and S. Guillou. Characterization of the vertical evolution of the three-dimensional turbulence for fatigue design of tidal turbines. Philosophical Transactions of the Royal Society A, 378(20190495), 2020b. URL http://dx.doi.org/10.1098/rsta.2019.0495. 1, 2.1, 2.1, 2.2, 2.2, 4

M. Thiébaut, J.-F. Filipot, C. Maisondieu, G. Damblas, A. Pieterse, R. Duarte, E. Droniou, N. Chaplain, and S. Guillou. Assessing the turbulent kinetic energy budget in an energetic tidal flow from coupled ADCPs measurements. Philosophical Transactions of the Royal Society A, 2020c. URL https://doi.org/10.1098/rsta.2019.0496. 1, 2.2, 2.2, 2.2, 4

J. Thiébot, N. Guillou, S. Guillou, A. Good, and M. Lewis. Wake field study of tidal turbines under realistic flow conditions. Renewable Energy, 151:1196–1208, 2020. URL https://doi.org/10.1016/j.renene.2019.11.129. 1

J. Thomson, B. Polagye, M. RIchmond, and V. Durgesh. Quantifying turbulence for tidal power applications. In OCEANS 2010 MTS/IEEE SEATTLE, pages 1–8, 2010. URL https://doi.org/10.1109/OCEANS.2010.5664600. 1

M. Togneri, D. Jones, S. Neill, M. Lewis, S. Ward, M. Piano, and I. Masters. Comparison of 4- and 5-beam acoustic doppler current profiler configurations for measurement of turbulent kinetic energy. Energy Procedia, 125:260–267, 2017a. URL https://doi.org/10.1016/j.egypro.2017.08.170. 1

M. Togneri, M. Lewis, S. Neill, and I. Masters. Comparison of adcp observations and 3d model simulations of turbulence at a tidal energy site. Renewable Energy, 114:273–282, 2017b. 1

T. Tokyay, G. Constantinescu, and J.A. Gonzalez-Castro. Investigation of two elemental error sources in boat-mounted acoustic Doppler current profiler measurements by large eddy simulation. Journal of Hydraulic Engineering, 135:875–887, 2009. URL https://doi.org/10.1061/(ASCE)HY.1943-7900.0000083. 1

B. Vermeulen, A.J.F. Hoitink, and M.G. Sassi. Coupled ADCPs can yield complete Reynolds stress tensor profiles in geophysical surface flows. Geophysical Research Letters, 38(L06406), 2011. URL https://doi.org/10.1029/2011GL046684. 1, 2.2, 2.2, 3, 3.1, 4

E. Zangiabadi, M. Edmunds, I.A. Fairley, M. Togneri, A.J. Williams, I. Masters, and N. Croft. Computational fluid dynamics and visualisation of coastal flows in tidal channels supporting ocean energy development. Energies, 8:5997–6012, 2015. URL https://doi.org/doi:10.3390/en8065997. 1